SEMARAK ILMU PUBLISHING

Journal of Advanced Research in Fluid Mechanics and Thermal Sciences

Journal homepage:
https://semarakilmu.com.my/journals/index.php/fluid_mechanics_thermal_sciences/index
ISSN: 2289-7879

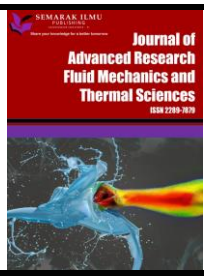

Aerodynamic Characteristics of Blerak Winglet

Mohamed Hussain Farook[1,*], Vishnu Kumar Gettin Chitharanjan[1]

[1] Department of Aeronautical Engineering, Hindustan Institute of Technology & Science, Chennai, 603103, Tamil Nadu, India

ARTICLE INFO

Article history:
Received 3 October 2022
Received in revised form 19 January 2023
Accepted 26 January 2023
Available online 19 February 2023

Keywords:
Aerodynamic performance; BLERAKE winglet; ANSYS Fluent; Computational Fluid Dynamics (CFD); lift and drag coefficient

ABSTRACT

The induced drag created by wingtip vortices has a significant impact on aircraft performance. Winglets are wingtip extensions that are intended to reduce the creation of vortices and increase the fuel efficiency. The present study is based on analyzing different winglets planform for aircraft at various angles of attack (AOA) to improve the aerodynamic efficiency. The Finite Volume Method in pressure-based solver along with the Realizable k - ε turbulence model, with standard atmospheric boundary conditions is used to do the CFD computations in ANSYS Fluent. According to the findings, an optimized BLERAK (Blended + Raked) winglet from the present study has a substantial impact on aerodynamic efficiency when compared to conventional winglets, and it is projected to yield a higher lift-to-drag ratio. The blerak winglets model gives 1.5 to 2% drag reduction than the other winglet models at angle of attack variations of 8°, 12° and 16°.

1. Introduction

The amount of aerodynamic drag that a body produces depends on variety of factors. Drag is influenced by an object's size, form, and inclination as well as by the airflow conditions passing through it. A three-dimensional drag of the lift distribution across the wing is induced drag. The quantity of drag is influenced by flow at the wing tips due to tip vortices. Long, thin slender wings are seen to have little induced drag. Elliptical planform wings have lower induced drag than rectangular planform wings, according to the Oswald's efficiency factor in the induced drag equation. The elliptic-shaped wings of the British Spitfire during World War II contributed to the aircraft's exceptional aerodynamic performance by reducing generated drag to an extremely low level. For a long time, wing designers have worked to lessen the amount of generated drag by giving the wing tips a unique shape. Based on the findings of the wind tunnel, the Wright Brothers incorporated curved trailing edges on their rectangular wings. The wing tips of contemporary aeroplanes are frequently twisted upward to create winglets. Richard Whitcomb of the NASA Langley Research Center tested and computer-analyzed winglets in a wind tunnel in the middle of the 1970s. The purpose of the winglet is to lessen the intensity of the tip vortex, resulting in a more two-dimensional flow over the wing. In flight testing at the NASA Dryden Flight Research Center, it was discovered that employing winglets

* *Corresponding author.*
E-mail address: hussainiman07@gmail.com

https://doi.org/10.37934/arfmts.103.2.4054

reduced fuel consumption of an aircraft of the Boeing 707 type by 6.5%. Richard Whitcomb's [1,2] design represents a winglet for large, heavy aircraft for the first time was given significant consideration. He projected that winglets would results in an increase in cruise economy of more than 7%. Further research was conducted and confirmed through tests. It is an extension at the end of each wing, either vertical or angled. Winglets increase efficiency by dispersing the shed wingtip vortex, which lowers the drag from lift and raises the lift-to-drag ratio of the wing. Winglets boost a wing's aspect ratio without noticeably raising the requisite weight and structural stress of the wing's structure. Blended winglets with airfoil NACA 65_3218 on a rectangular wing were analysed to assess the performance of winglets at Cant angles and to compare aerodynamic properties 0°, 30°, 45°, 60° at different angle of attack. The experiment investigation was brought out with help of closed-loop wind tunnel settings at sea level with a 35 m/s wind speed. ANSYS CFX solver used for CFD simulations at low subsonic flow speed. By comparison of both CFD and wind tunnel results, it was concluded that the cant angle 45° provided more lift contrast to other winglet design. But outcomes of the wind tunnel shows that winglet at cant angle 60° generated12% less lift than with a cant angle, winglet 45˚. This results from CFD simulation results are not similar to the wind tunnel results due to the disparity of mesh quality [3].

Solid Works was used for the design of NACA 2411, NACA 0010, and NACA 0012, which underwent flow simulation. The NACA 2411, which has wing proportions similar to those of the Airbus A320, was selected as having the best aerodynamic performance. The simulation was carried out in Blended, Raked and Fence type winglet. These winglets were studied and simulated in STAR CCM+ to result by adding winglet to the wing increasing the aerodynamic ability. In the outcomes of a raked winglet was found with higher efficiency than others. In order to increase the efficiency, the raked and blended winglets are modified into 5 blended winglets and 5 raked winglets totally 10 winglets designed. According to the findings of the wing's CFD research, the wing with blended winglet type 2 has the highest efficiency in terms of C_L/C_D. The improvement of efficiency was 5.57% [4]. The optimal performance of a subsonic aircraft wing's aerodynamics at different winglet cant angles has been investigated through numerical research. The NACA65_3218 airfoil section coordinates for the composite design of the wing and the winglet are included in the analysis. The binary and experimental studies in the current work are found to be fairly in agreement. This study's blended winglets are positioned at various angles along the wing were 30°, 45°, 60°, and 90°. For the purpose of determining and estimating the aerodynamic properties of a three-dimensional subsonic rectangular wing, a numerical validation approach using the CFD programme 6.3.26 Fluent and a Spalart-Allmaras turbulence model is provided (with NACA65_3218airfoil section). According to the findings, a wing with winglets can enhance the lift to drag ratio was roughly 6 to 15% higher than a wing without winglets. When compared to a wing without winglets, the (L/D) was enhanced by around 3 to 15%. The winglet improves the (L/D) ratio than a conventional model [5].

The various wingtip device geometries are presented and investigated under various flight conditions, and the effects of various geometrical parameters on the forces of lift and drag are evaluated. It is done using potential flow-based panel method studies, computational fluid dynamic models, and an effort at experimental observations. The major findings of this study suggest that it is feasible to boost a given wing's aerodynamic efficiency by 10% for a number of wingtip device combinations. Some of the designs used might enhance the lift-to-drag ratio, or L/D, by 10%. This would lead to an increase in range and endurance as well as a reduction in the length of the takeoff field and the distance needed to land using a ground-roll [6]. The leading-edge spot on the airfoil that has the most curvature. The point of greatest curvature is known as the trailing edge and is located near the back of the airfoil. The chord line linking the airfoil's trailing and leading-edge locations. AOA is the angle formed by the direction of air velocity and the wing chord line [6]. In this investigation, it

was determined how much a catamaran seaplane floats due to its hull form. The twin float's total fluid resistance was predicted using numerical modelling, and interference phenomena was also studied. The findings are verified using currently available experimental data that has already been examined. The prediction of hull resistance uses CFDSOF. It was picked due to its open-source nature and online training capabilities. With the Operating Empty Weight (OEW) of an Indonesian Aerospace (IAe) N219 aircraft, a numerical simulation of a catamaran seaplane float model with symmetric demi-hull and three variants of hull separation was performed. With a Froude number range of 0.40 to 0.75, simulations were run on the model. With an 8% mesh convergence error, a mesh with 400 000 cells has been selected [7]. An analytical thermodynamic combustion model is developed in MATLAB/Simulink for the Rotax 912 S/ULS engine to simulate the generated torque and power values, as well as fuel consumption with altitude capabilities [8]. As stated in this research, engine modifications can also boost fuel economy at higher altitudes, in addition to wing and winglet modifications. With an incidence angle of 15° and a flow Reynolds number of $1.0x10^5$, the numerical simulation of turbulent flow at the delta wing suction face with an apex angle of 80° was conducted. The suction face of the delta wing, where the grid density is rather finely tuned, is where the pressure distribution under the apex vortex originated. Near point x/c=0.25, which is extremely close to the wing apex, the defect pressure coefficient -Cp is at its highest value. The flow is most depressed towards the apex and becomes less depressed as it moves towards the trailing edge of the delta wing [9]. When a circular vortex generator and a triangle vortex generator are used to modify an airfoil, the circular vortex generator's vorticities are greater than those of the triangular vortex generator because the circular vortex generator separates the flow better. For circular and triangular vortex generators, the lift to drag ratio is enhanced by 3.65% and 3.54%, respectively [10]. By evaluating the Savonius wind turbine's functionality and contrasting the torque and power production of various rotor diameters at a fixed wind speed. All models' power coefficients rise with TSR, and the best efficiency is often seen at close to unity (0.9) TSR. Model 2 generated the highest power coefficient when compared to the other two Savonius wind turbine models, followed by Model 3 and Model 1, respectively, with 0.75m height and 0.3m diameter [11].

As a cooling fluid, the simulation is run using both pure water and water containing nanoparticles [12]. To test the 2D modelling, the behaviour of thermohydraulic properties of the convective heat transfer flow via pipes, Al2O3 nanoparticles are introduced to water as a base fluid. The numerical outcomes showed that adding nanoparticles to the fluid enhanced heat transfer and the flow's Nusselt number. The multiple tip-4 winglet is best at improving lift coefficient, although multiple tip-3 outperforms it in terms of lift to drag ratio. The baseline wings function best when the aspect ratio is greater. Overall, it is discovered that winglets are more efficient at lower aspect ratios and that a moderate aspect ratio of 10 offers the greatest increase in aerodynamic efficiency [13]. In order to reduce interference drag at the wing/winglet junction, a blended winglet is linked to the wing with a smooth curve rather than a sharp angle. A vortex that increases drag and negates some of the benefits of the winglet can be created in this area by a steep interior angle that interacts with the boundary layer flow. For business jets and sailplanes, when customer preference is a crucial marketing factor, the blended winglet is employed [14]. Instead of lowering fuel consumption, the installation of the gadget can be utilised to expand the airplane's payload/range capacity. Drag during take-off and landing is significantly reduced in aircraft having blended winglets [16].

From the review of literature survey, we can infer that further scope of the winglet can be analysed by combining multiple winglets and modification in the winglets. Hence it can be further improved for structural modification to get better efficiency. An increase in the rotor component's angle of attack led to an increase in drag of around 34% to 45%, while the fuselage component was responsible for about 55% to 65% of the drag increase. Also, a considerable overall pressure value

from -235 Pa to 250 Pa displayed along the reduced model helicopter clearly revealed that the geometry's complexity led to unfavourable pressure [18].

A test without Boundary Layer Control was performed on the model with 20 pressure tappings, and the point of flow separation was recorded. Eventually, the model's blowing and suction holes were appropriately shaped, and a compressor/vacuum pump was added to regulate the boundary layer and examine its impact on the performance of the NACA 0021 aerofoil. Both Boundary Layer Control approaches provide an improvement in the maximum lift coefficient [19]. The lift coefficient values for the Serindit V-2 UAV aircraft are CL_o=0.36 and CLMax = 1.42 at an angle of 13^o, to calculate the values of flow characteristics such as coefficient of drag, lift, moment, and pressure distribution based on fluid flow that occurs in the aircraft with variations in Angle of Attack and air velocity [20]. With a CD_o of 0.05 was achieved. Whereas the computational fluid dynamics numerical simulation yielded a CM_o value of -8.34 x 10-5. Using the response surface approach, the experimental results of the flapping wing micro air vehicle design were examined. The results showed that the flapping wing mechanism had aerodynamic characteristics of 15% at 4.29 m/s, and 9 Hz [21]. The unusual behaviour of the drag coefficient in the transonic region at large elongations was observed through computational studies. The aerodynamic properties of the aircraft with variable elongation are impacted by the drag coefficient of the plate increasing as elongation decreases. For Mach values between 0.06 and 4 [22]. The various types of winglets are used in commercial aircraft is shown in Figure 1.

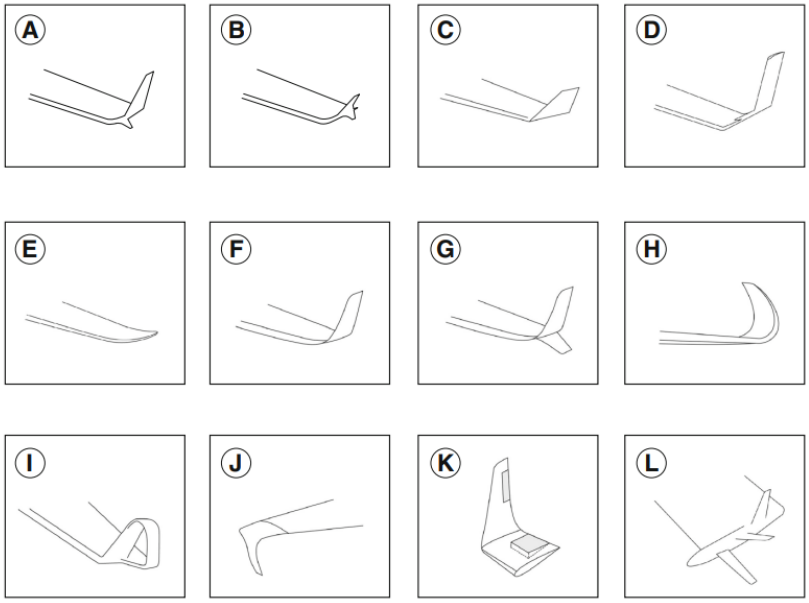

Fig. 1. (a) Whitcomb (b) Tip fence (c) Canted winglet (d) Vortex diffuser (e) Raked winglet (f) Blended winglet (g) Split winglet (h) Sharklet (i) Spiroid winglet (j) Downward canted (k) Active winglets (l) Tip sails

2. Formulation of the Problem

To increase the L/D ratio, optimization of the winglet can be analysed. Further the winglet will be validated with the baseline conventional model. The simulation will be carried out for wing with modified winglets. Finally, the optimized model from the present study will be compared with other existing literature studies.

For the prediction of wing aerodynamics, the Realizable k - ε model will capture the turbulence compared to the conventional k - ε model, the realizable k - ε model vary from one other in two key areas

i. The turbulent viscosity has a different expression in the realizable k - ε model.
ii. Using a precise equation for the mean-square vorticity fluctuation's conveyance, a modified transport equation for the dissipation rate, ε, has been created [15].

When a model is said to be "realizable," it indicates that it complies with specific mathematical restrictions on the Reynolds stresses that are in line with the physics of turbulent flows. The conventional k - ε model and the RNG k - ε model are both unrealizable.

Transport Equations for the Realizable k-ε Model:

$$\frac{\partial}{\partial t}(\rho k) + \frac{\partial}{\partial x_j}(\rho k u_j) = \frac{\partial}{\partial x_j}\left[\left(\mu + \frac{\mu_t}{\sigma_k}\right)\frac{\partial k}{\partial x_j}\right] + G_k + G_b - \rho\epsilon - Y_M + S_k \tag{3}$$

and

$$\frac{\partial}{\partial t}(\rho \epsilon) + \frac{\partial}{\partial x_j}(\rho \epsilon u_j) = \frac{\partial}{\partial x_j}\left[\left(\mu + \frac{\mu_t}{\sigma_\epsilon}\right)\frac{\partial \epsilon}{\partial x_j}\right] + \rho C_1 S_\varepsilon - \rho C_2 \frac{\varepsilon^2}{k+\sqrt{\nu\varepsilon}} + C_{1\varepsilon}\frac{\varepsilon}{k}c_{3\varepsilon}G_b + S_\epsilon \tag{4}$$

where

$$c_1 = max\left[0.43, \frac{\eta}{\eta+5}\right], \eta = S\frac{k}{\varepsilon}, S = \sqrt{2s_{ij}s_{ij}} \tag{5}$$

These equations use the term G_k to denote the turbulence's kinetic energy production as a result of mean velocity gradients. G_b is the buoyancy-induced creation of kinetic turbulence energy. The variable dilatation in compressible turbulence is represented by Y_M as a contribution to the total dissipation rate. Constants $C_{1\varepsilon}$ and C_2 exist. The turbulent Prandtl numbers for k and ε are denoted by σ_k and σ_ϵ, whereas S_k and S_ϵ are the user-defined source terms as per reference [9].

3. Methodology

The analysis is performed on three shapes of winglets: blended, raked and blerak. To determine the significance of a winglet, the results of these comparisons are made with wings without winglets. The Ansys Fluent Solver is used to do the CFD simulation for an angle of attack range of (0°- 16°) with 4° as increment for all models in low subsonic flow with Reynolds Number of 616218 at standard atmospheric condition is observed.

3.1 Geometry and Modelling

In Solid Works, the wing and winglets were designed using the profile from the NACA six-digit series of 65_3218, as shown in Figure 2. The chord and semi-wing spans were set to 300 mm and 1591.5 mm in each case respectively as per the reference [6]. The winglets ant angle 45° for height of 155 mm with a sweep of 25% of conventional winglet is shown in Figure 3.

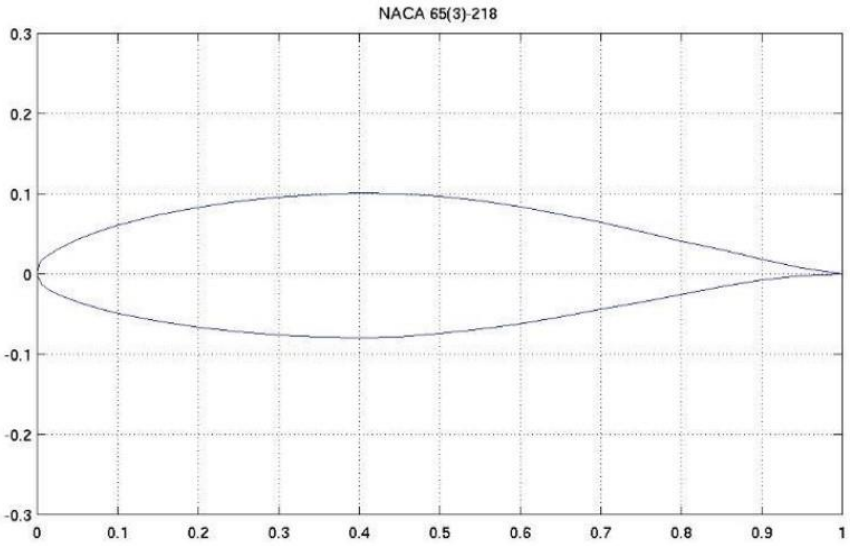

Fig. 2. Profile of NACA 65_3218

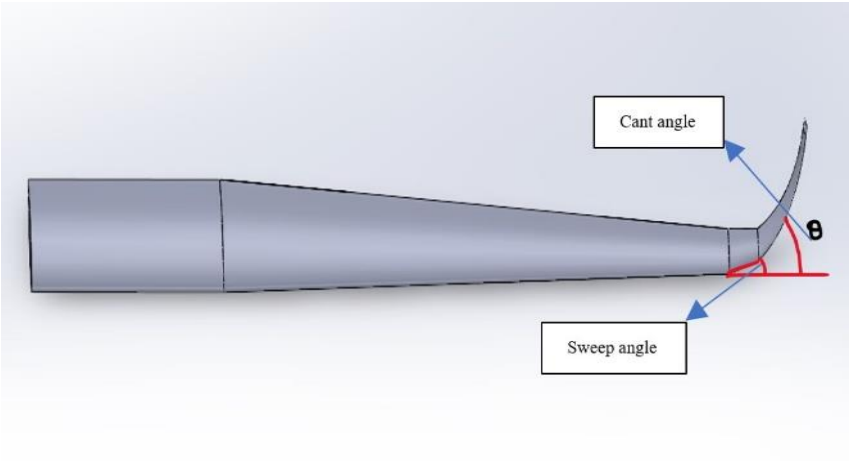

Fig. 3. Winglet condition of NACA 65_3218

S. No:	Wing Type	Cant Angle (θ)	Winglet Sweep Angle (ϕ)
1.	Conventional	0	-
2.	Raked	-	27°
3.	Blended	30° & 45°	-
4.	Blerak	30°& 45°	27°

The condition for the Blerak winglet were kept consistent with sweep angle of 27° of the conventional wingtip chord variations in blended winglet. The conventional wing, Raked winglet and Blended winglets are shown in Figure 4(a)-(d). The cant angle (θ) 30° and 45° as shown in Figure 4(e) and (f).

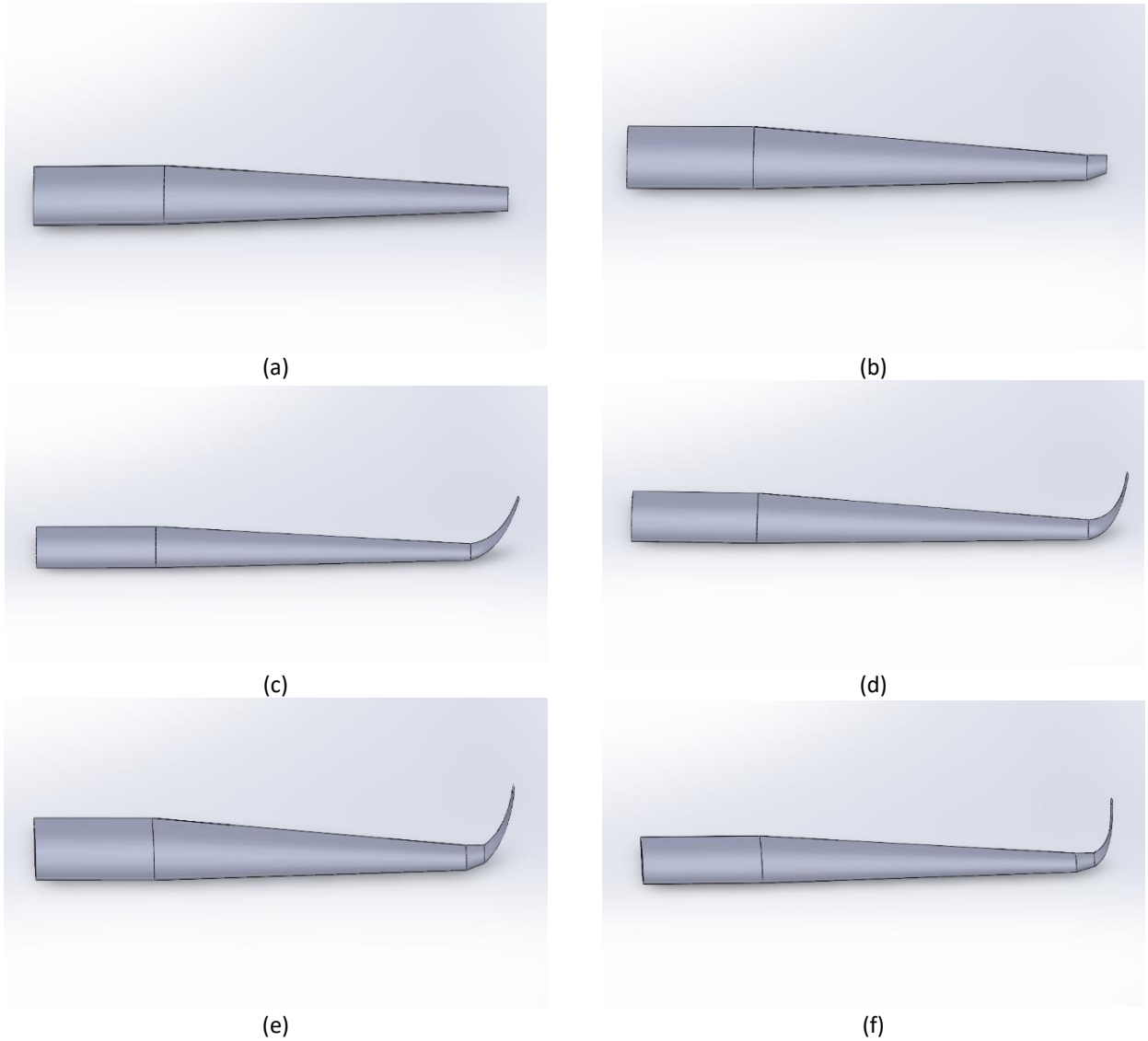

Fig. 4. (a) Conventional wing (b) Raked wing (c) Blended winglet 30° (d) Blended winglet 45° (e) Blerak winglet 30° (f) Blerak winglet 45°

5. Results and Discussion

ANSYS R19.2 Workbench is used to analyse the results. The domain is created for performing simulations for various grid resolutions, for the number of elements, a grid refinement study was carried out as shown in Figure 5. ANSYS Workbench was used to create a 3-D unstructured tetrahedral mesh with inflation layers all around the geometry as shown in Figure 6. The surface mesh over the wing with winglet section is shown in Figure 7. The mesh element size was smaller near the wing and winglet, and it gradually expanded as it got closer to the domain border walls. This was done in order to determine the right range for grid independent study. From Table 1, the mesh is varied between 3.1 and 5.4 million elements, which is quite sufficient in terms of calculation time and output quality. A layer of structured grids was created by applying an inflation layer to the mesh geometry to capture the flow over the air foil's boundary. The inflating layer was assumed to be the first inflation layer thickness y plus wall spacing as shown in Figure 8.

Table 1
Grid independent study

Velocity	Aerodynamic Coefficients	Elements 304783	Elements 4237837	Elements 5167452	Helal *et al.,* [5] 4703836	Error (%)
30 m/s	C_L	0.1268	0.1306	0.1361	0.1287	1.45
	C_D	0.0186	0.0192	0.0127	0.0477	1.48

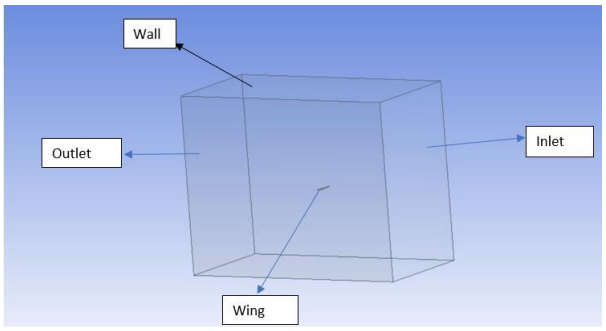

Fig. 5. Rectangular domain

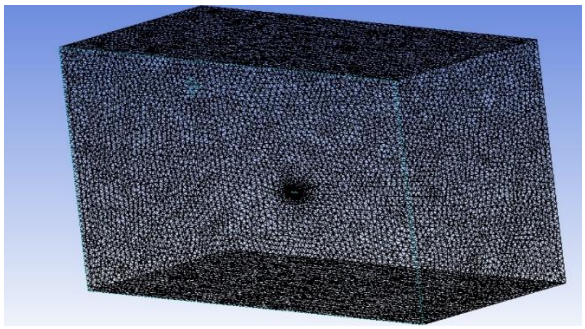

Fig. 6. Mesh around the winglet

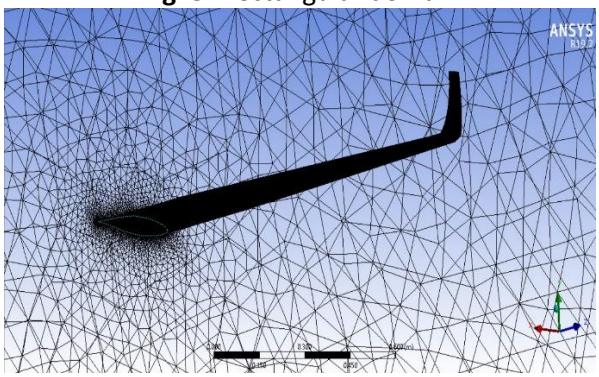

Fig. 7. Mesh near edge of the wing

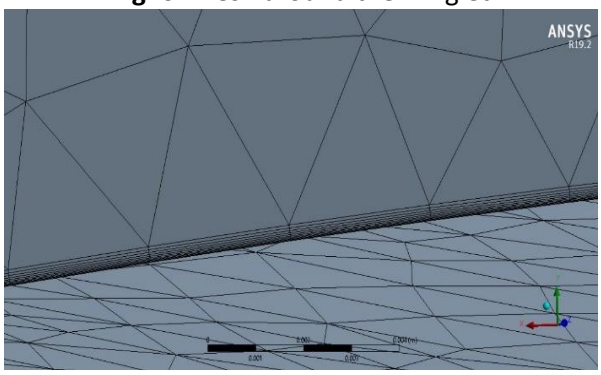

Fig. 8. Inflation layer near edge of the wing

The FLUENT solver has performed computational simulations utilizing the finite volume technique and a pressure-based solver at steady state. The material air-ideal gas is taken into consideration and SIMPLE algorithm is chosen. The kinematic eddy turbulent viscosity modelled transport calculation is solved by two-equation, k-epsilon model. The k-epsilon Realizable model has enhanced in ANSYS Fluent with a y+ careless wall treatment (Enhanced Wall Treatment), allowing model to be applied regardless of the near wall y+ resolution. All of the walls are operated at sea level pressure and temperature under adiabatic wall conditions. The inflow velocity and initial wall temperature are given. An outflow boundary condition is defined at the exit. No slip boundary condition is imposed at solid walls. The working fluid was decided upon as being ideal gas. The inlet speed is assumed to be 30 m/s. For the numerical simulation, the boundary conditions listed below in Table 2 were employed.

In the present study the variation of the model for different winglet types such as raked blended and blerak, the results of the rectangular tapered wing of NACA 65_3218 airfoil are compared to one another. This research examines the aerodynamic properties including lift and drag coefficient, lift/drag ratio, and tip vortices. At a velocity of 30 m/s, Table 3 illustrates how the lift coefficient varies with angle of attack for all winglet and conventional rectangular wing configurations.

Table 2
Boundary conditions

Parameters	Standard conditions
Pressure	101325 Pa
Temperature	288.2 K
Velocity	30 m/s
Viscosity	1.7894 x 10^{-5} Kg/m s
Density	1.225 Kg/m^3
Mesh	Tetrahedrons
Solver	Pressure based
Turbulence model	K-epsilon, Realizable model
No slip wall	Wing with and without winglets
Domain	Rectangular domain
Taper Ratio	0.4
Reynolds Number, Re	6.1x10^5

Table 3
Angle of attack vs lift coefficient

AOA	conventional	Raked	Blended 30°	Blerake 30°	Blended 45°	Blerake 45°
0°	0.1361	0.1465	0.1454	0.1471	0.1432	0.1427
4°	0.2604	0.2753	0.2772	0.2798	0.2763	0.2750
8°	0.3831	0.4006	0.4043	0.4149	0.4077	0.4071
12°	0.5165	0.5218	0.5240	0.5298	0.5295	0.5279
16°	0.6654	0.6784	0.6826	0.6862	0.6975	0.6954
18°	0.4576	0.4556	0.4182	0.3837	0.4445	0.3712

For the winglets, constructed in the present study the drag coefficient versus with angle of attack is plotted in Table 4. It can be observed that, the drag coefficient increases as the angle of attack increases.

Table 4
Angle of attack vs drag coefficient

AOA	conventional	Raked	Blended 30°	Blerake 30°	Blended 45°	Blerake 45°
0°	0.0190	0.0185	0.0203	0.0200	0.0199	0.0202
4°	0.0239	0.0233	0.0248	0.0251	0.0249	0.0250
8°	0.0364	0.0353	0.0343	0.0342	0.0357	0.0356
12°	0.0439	0.0436	0.0434	0.0433	0.0445	0.0444
16°	0.0559	0.0551	0.0535	0.0513	0.0491	0.0487
18°	0.0712	0.0823	0.0741	0.0732	0.0821	0.0750

Table 5 illustrates the lift to drag coefficient varies with angle of attack for winglets in the present study with the conventional rectangular wing configurations.

Table 5
C_L/C_D versus angle of attack

AOA	conventional	Raked	Blended 30°	Blerake 30°	Blended 45°	Blerake 45°
0°	7.1519	7.8982	7.1733	7.3635	7.1936	7.0772
4°	10.9092	11.8023	11.1558	11.1763	11.1540	11.0065
8°	10.5288	11.3575	11.8007	12.1466	11.4152	11.4474
12°	11.7559	11.9752	12.0770	12.2314	11.8968	11.8845
16°	11.9110	12.3071	12.7572	13.3811	14.2007	14.2654
18°	6.4270	5.5358	5.6432	5.2417	5.441	4.9493

The lift to drag ratio of the conventional wing from the literature survey [12,17,15] is validated with the present study as shown in Figure 9.

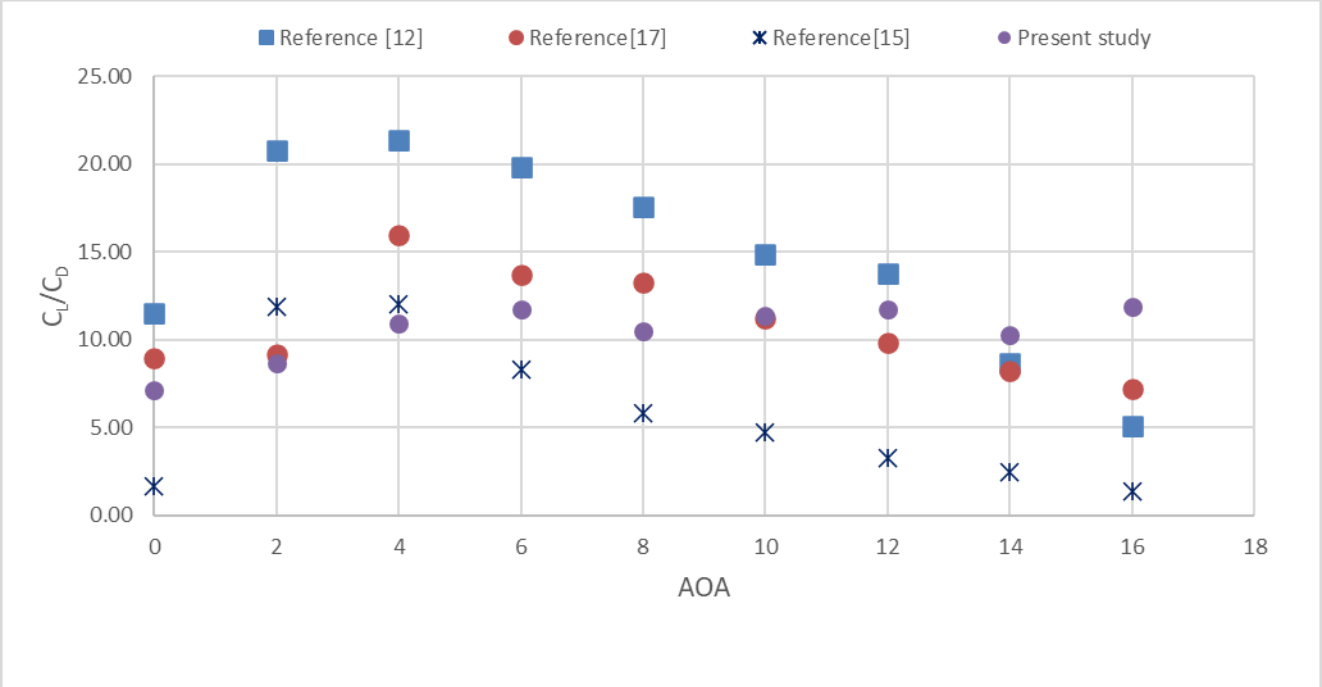

Fig. 9. Validation of C_L/C_D Vs AOA for the conventional model

Table 3 show that when the angle of attack increases, the lift also rises. The lift coefficient, CL, of wings with winglets is higher than that of wings without winglets depending on the angle of attack. At angles of attack of 4 and 8 degrees, the blended and raked winglet has the maximum lift coefficient followed by the blerak 30° and blerak 45° is shown in Figure 10.

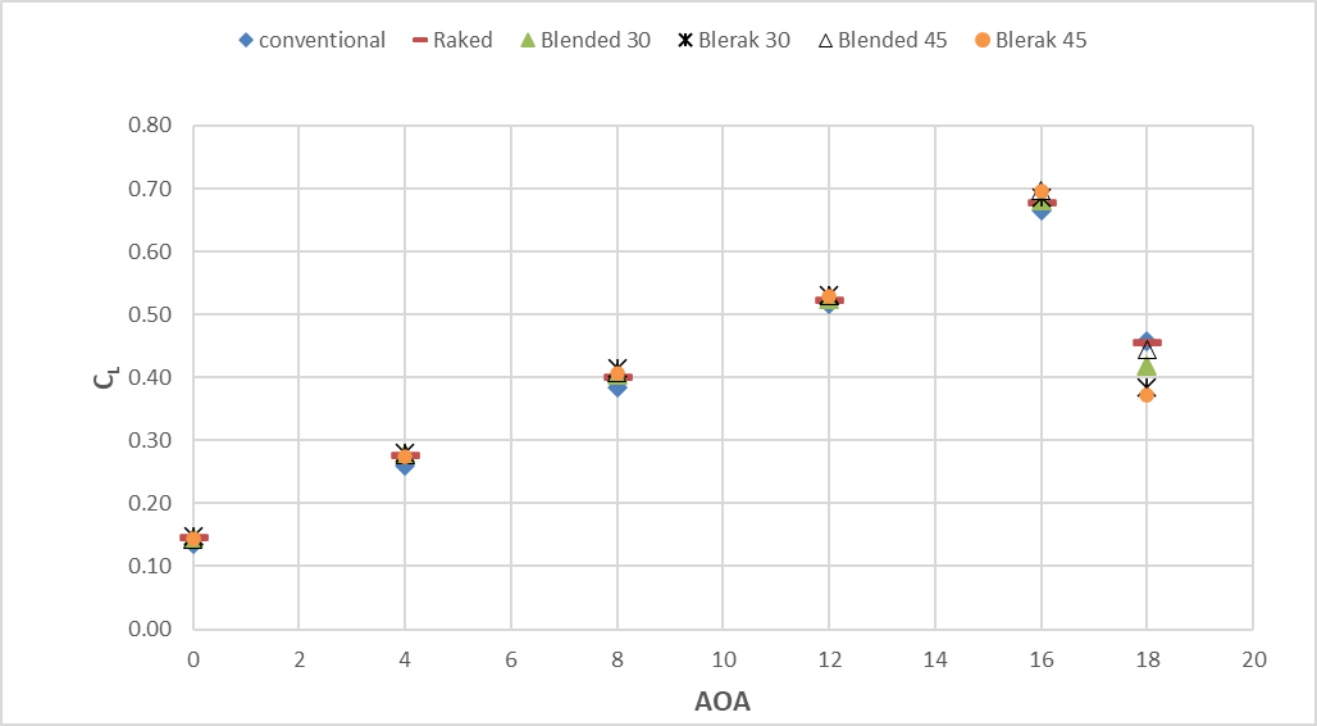

Fig. 10. C_L vs AOA for various winglets in present study

The effect of wings with different winglets is not significant at 0 degrees angle of attack due to low induced drag and the wings with winglets have more surface area, which caused the friction drag to increase. From the Table 4, the drag increases with the increase of the angle of attack. When the angle of attack is high, the drag increases and is then reduced by the winglets. When compared to a wing without winglets, it was observed that the blerak 45° has the lowest drag coefficient; CD, with angle of attack. The blerak 30° has the second-lowest drag coefficient, CD, with angle of attack is shown in Figure 11.

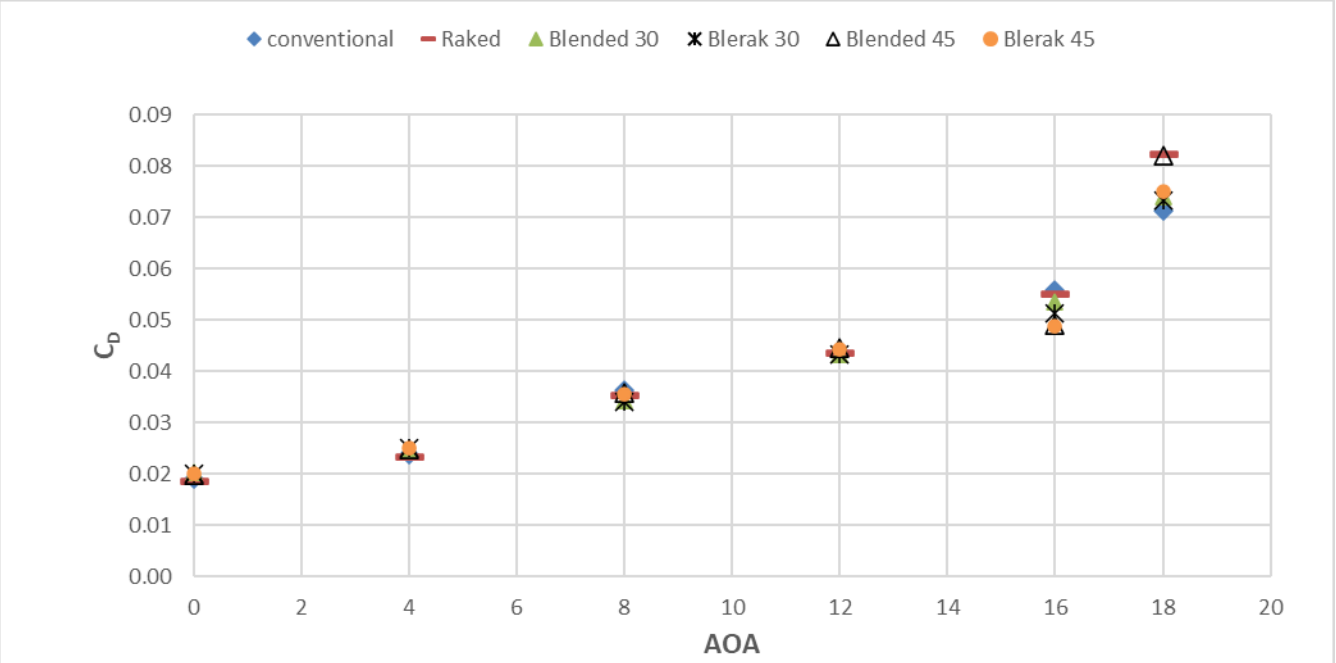

Fig. 11. C_D Vs AOA for various winglets in present study

Wings with winglets have a greater lift-to-drag ratio than wings without winglet, as demonstrated in Table 5. When compared to wings without winglets, the blerak 45° has the greatest lift-to-drag ratio, or CL/CD along angle of attack. The second-highest lift-to-drag ratio, or CL/CD, combined with angle of attack as compared to the wing without winglets is achieved by the blerak 30° is shown in Figure 12. The third lowest lift-to-drag ratio, CL/CD with angle of attack compared to wing without winglet is observed by the blended and raked winglet shape.

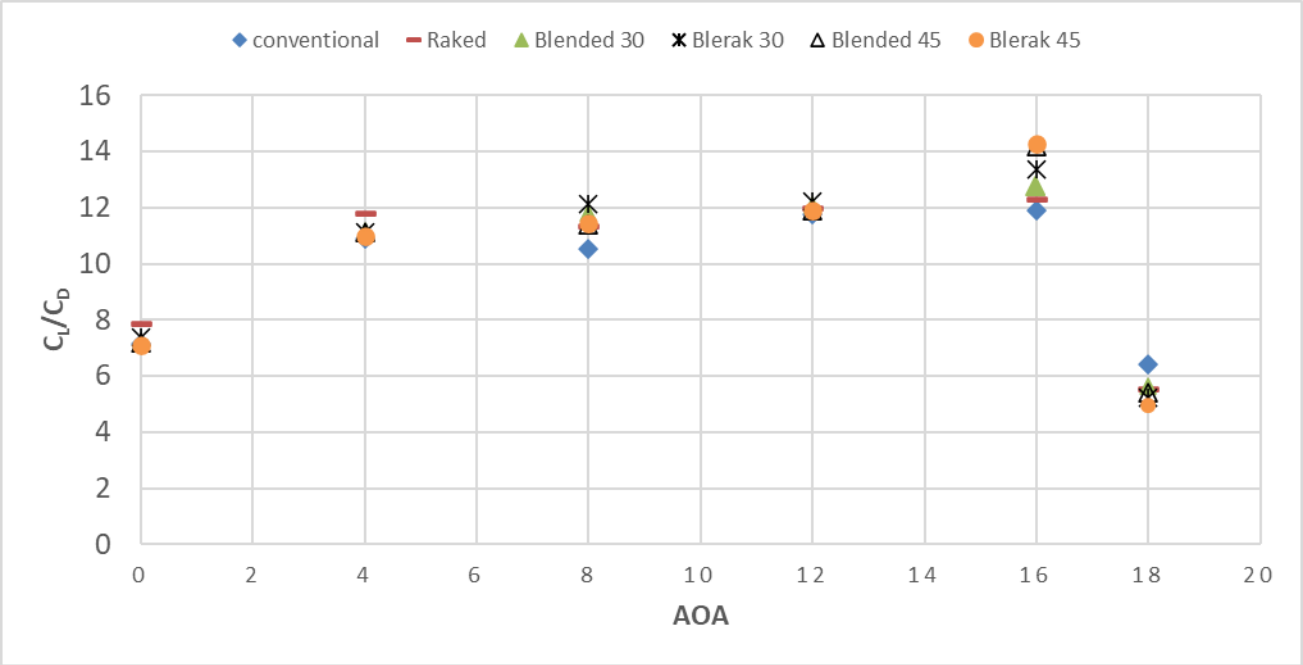

Fig. 12. C_L/C_D Vs AOA for various winglets in present study

When compared to wings without winglets, the blerak 45° has the greatest lift-to-drag ratio, or CL/CD along angle of attack. From Table 6, the efficiency of drag is shown for blerak model winglets compared with the conventional model.

Table 6
Summary of drag coefficient

Angle of Attack(α)	C_D	C_D winglets models			
	Conventional	blerake 30	Drag reduction (%)	blerake 45	Drag reduction (%)
0	0.0190	0.0200	0.95	0.0202	0.94
4	0.0239	0.0251	0.94	0.0250	0.95
8	0.0364	0.0342	1.06	0.0356	1.02
12	0.0439	0.0433	1.01	0.0444	1.00
16	0.0559	0.0513	1.10	0.0487	1.14

Figure 13, depicts the contours of the static pressure for a winglet. The upper surface will provide a lower static pressure at an angle of attack of 0 degrees. When the Cant angle(θ) increases and the pressure becomes more uniform, the pressure losses resulting from the connection between the wing and the winglet diminish, which reduces drag. The pressure at upper surface decreases at an angle of attack of 12 degrees, but lift is still capable of being generated; nevertheless, the majority of the total force is directed backward as drag. The velocity is increased at the lower pressure region of the wing with winglet as shown in Figure 14.

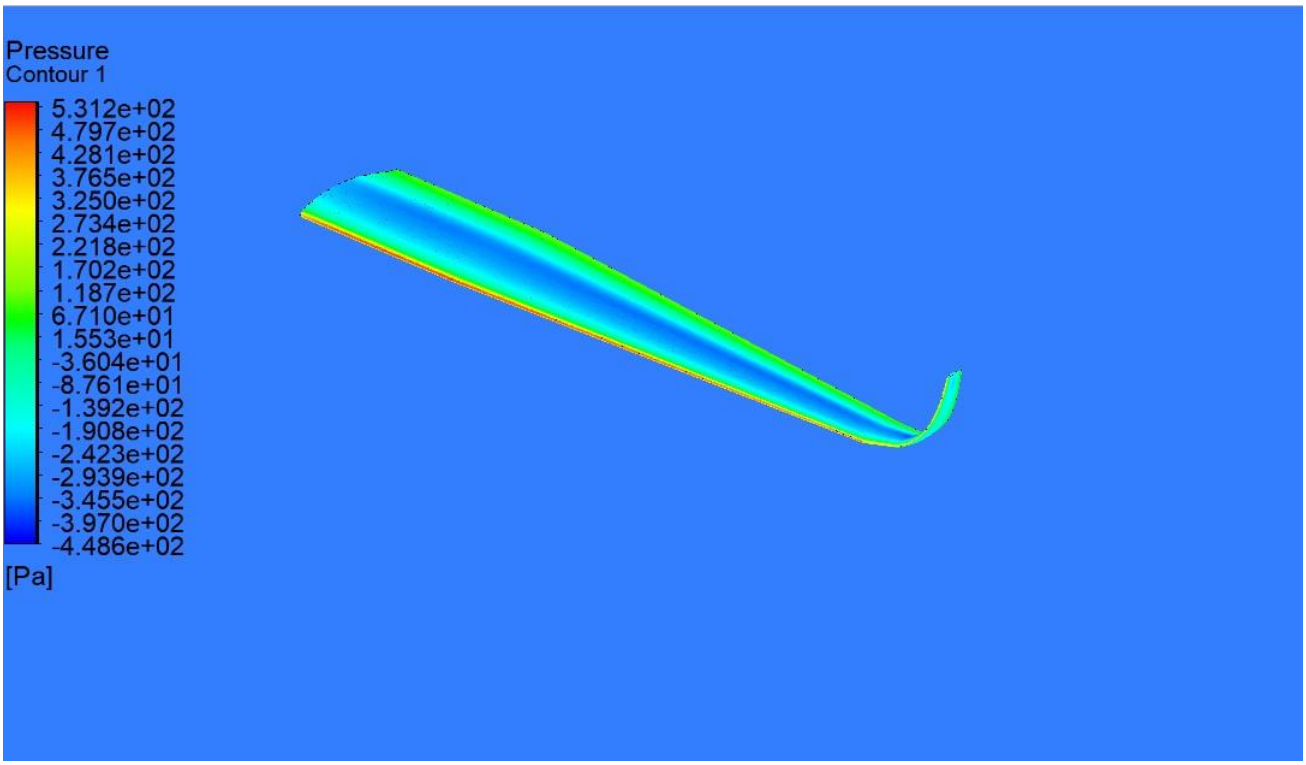

Fig. 13. Pressure contours for Blerak winglet

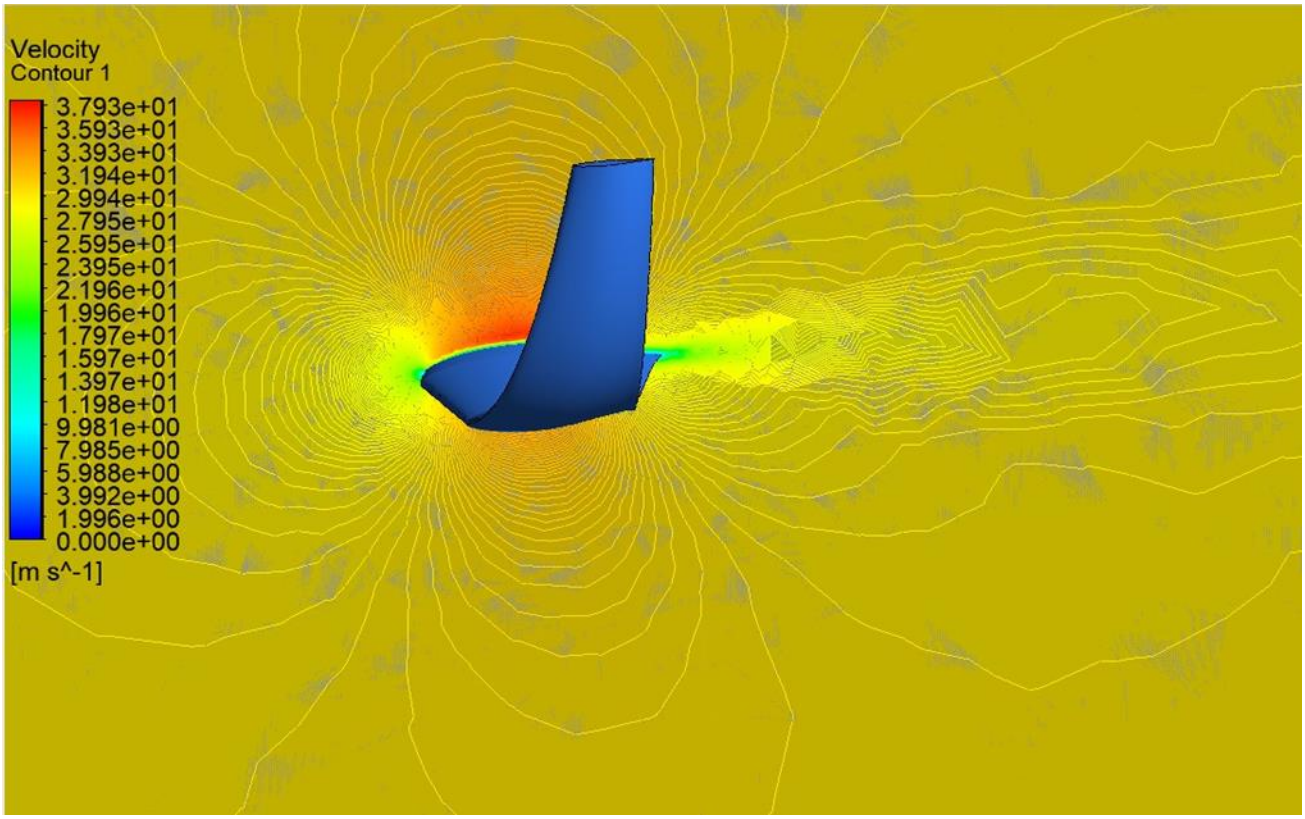

Fig. 14. Velocity contours for Blerak winglet

6. Conclusions

This research uses the finite volume method to examine a 3D wing with and without winglets in three cases such as raked, blended, and blerak winglets. When winglets are installed, it is shown that the lift coefficient value for blerak winglets increases and the drag coefficient decreases at various angles of attack, and the lift to drag ratio increases compared to other models, especially with the blended winglet. Raked winglets also produces the better lift coefficient than the conventional wing but the blended winglets produce higher L/D ratio than the raked at an AOA 8°, 12° and 16°. Eventually, conventional and raked winglets are having less L/D ratio when compared with blerak models. The blerak winglets model gives better drag reduction than the other model at angle of attack 8°, 12° and 16°. These blerak model differences were almost near to the blended winglets. Herewith, it has been concluded that the winglets blerak model and the blended model are similar in terms of aerodynamic conditions.

7. Future Scope

Despite reaching important results about the exploits and effects by considering wingtip devices from an aerodynamic angle, the scope of the research can be further be carried out in the following areas

i. Experimental measurements can be undertaken in order to compare the CFD simulations using a calibrated load cell to measure precisely.
ii. The analysis can also be conducted in the water channel to observe the flow visualization using dye injection setup.
iii. Further modification of winglet is to fix propeller at the tip of the winglet to observe the interaction vortex fluctuations arising from the propeller and the wiglets.

Acknowledgement
This research was not funded by any grant.

References

[1] Whitcomb, Richard T. *A design approach and selected wind tunnel results at high subsonic speeds for wing-tip mounted winglets*. No. L-10908. 1976.
[2] Whitcomb, R. T., "Methods for Reducing Aerodynamic Drag", *NASA Conference Publication* 2211, Proceedings of Dryden Symposium, California 1981
[3] Beechook, Abhinivesh, and Jian Wang. "Aerodynamic analysis of variable cant angle winglets for improved aircraft performance." In *2013 19th International Conference on Automation and Computing*, pp. 1-6. IEEE, 2013.
[4] Quraishi, Mohd Mohiuddin, Mohd Abdul Razakh, and Shivasri Chithaluri. "Design and CFD Analysis of Parametric Winglets." *The SIJ Transactions on Advances in Space Research & Earth Exploration (ASREE)* 4 (2016): 7-14. https://doi.org/10.9756/SIJASREE/V4I2/04010020101
[5] Helal, H. S., Essam E. Khalil, Osama E. Abdellatif, and Gamal M. Elhariry. "Aerodynamic Analyses of Aircraft-Blended Winglet Performance." *IOSR J. Mech. Civ. Eng. Ver* 13, no. 3 (2016): 2320-334.
[6] Mosquera Alonso, Andrea. "Analysis of drag reduction in wingtip devices." Bachelor's thesis, 2017.
[7] Gunawan, Gunawan, Yanuar Yanuar, A. S. A. Utomo, M. F. Tjiptadi, and M. N. Luthfi. "Hull Water Resistance Calculation of a Seaplane Twin Float with Clearance Ratio Variation Configurations." *Journal of Advanced Research in Experimental Fluid Mechanics and Heat Transfer* 1, no. 1 (2020): 38-43.
[8] Otkur, Murat. "Altitude Performance and Fuel Consumption Modelling of Aircraft Piston Engine Rotax 912 S/ULS." *Journal of Advanced Research in Applied Sciences and Engineering Technology* 23, no. 1 (2021): 18-25. https://doi.org/10.37934/araset.23.1.1825

[9] Boumrar, Iddir, and Ridha Djebali. "Experimental validation of pressure distribution prediction under delta wing apex vortex at high Reynolds numbers." *CFD Letters* 11, no. 3 (2019): 92-102.
[10] Niknahad, Ali. "Numerical study and comparison of turbulent parameters of simple, triangular, and circular vortex generators equipped airfoil model." *Journal of Advanced Research in Numerical Heat Transfer* 8, no. 1 (2022): 1-18.
[11] Bajuri, Muhammad Nur Arham, Djamal Hissein Didane, Mahamat Issa Boukhari, and Bukhari Manshoor. "Computational Fluid Dynamics (CFD) Analysis of Different Sizes of Savonius Rotor Wind Turbine." *Journal of Advanced Research in Applied Mechanics* 94, no. 1 (2022): 7-12. https://doi.org/10.37934/aram.94.1.712
[12] Elfaghi, Abdulhafid MA, Alhadi A. Abosbaia, Munir FA Alkbir, and Abdoulhdi AB Omran. "CFD Simulation of Forced Convection Heat Transfer Enhancement in Pipe Using Al2O3/Water Nanofluid." *Journal of Advanced Research in Numerical Heat Transfer* 8, no. 1 (2022): 44-49. https://doi.org/10.37934/cfdl.14.9.118124
[13] Narayan, Gautham, and Bibin John. "Effect of winglets induced tip vortex structure on the performance of subsonic wings." *Aerospace Science and Technology* 58 (2016): 328-340. https://doi.org/10.1016/j.ast.2016.08.031
[14] McLean, Doug. "Wingtip devices: what they do and how they do it." In *Boeing performance and flight operations engineering conference*. 2005.
[15] Versteeg, Henk Kaarle, and Weeratunge Malalasekera. *An introduction to computational fluid dynamics: the finite volume method*. Pearson education, 2007.
[16] "Blended Winglets Improve Performance." Aero - blended winglets improve performance. The Boeing Company, 2009. https://www.boeing.com/commercial/aeromagazine/articles/qtr_03_09/article_03_1.html.
[17] Lambert, D. "Numerical Investigation of Blended Winglet Effects on Wing Performances, report." *Liege University* (2007).
[18] Othman, Nurain, Iskandar Shah Ishak, and Md Nizam Dahalan. "Static Analysis of Unsteady Aerodynamics Wake of Simplified Helicopter Model Via Simulation Work." *Journal of Advanced Research in Fluid Mechanics and Thermal Sciences* 89, no. 1 (2022): 142-153. https://doi.org/10.37934/arfmts.89.1.142153
[19] Ali, Jaffar Syed Mohamed, Mohd Farid Amran, and Nurul Aziz Mohamad. "Experimental Study on the Effect of Boundary Layer Control on the Aerodynamics Characteristics of NACA 0021 Aerofoil." *Journal of Advanced Research in Fluid Mechanics and Thermal Sciences* 94, no. 1 (2022): 129-137. https://doi.org/10.37934/arfmts.94.1.129137
[20] Anuar, Kaspul, and Agung Soegihin. "Aerodynamic Analysis of Unnamed Aerial Vehicle Serindit V-2 Using Computational Fluid Dynamics." *Journal of Advanced Research in Fluid Mechanics and Thermal Sciences* 93, no. 1 (2022): 83-93. https://doi.org/10.37934/arfmts.93.1.8393
[21] Yusoff, Hamid, Aliff Farhan Mohd Yamin, Siti Nur Amalina Mohd Halidi, Nor Suhada Abdullah, Halim Ghafar, Shafiq Suhaimi, Koay Mei Hyie, and Wan Mazlina Wan Mohamed. "The Optimisation of Aerodynamic Performance Enhancement of a Flapping Wing using Response Surface Methodology." *Journal of Advanced Research in Fluid Mechanics and Thermal Sciences* 91, no. 1 (2022): 69-82. https://doi.org/10.37934/arfmts.91.1.6982
[22] Alekseyenko, Serhii, Andrii Dreus, Mykola Dron, and Olexandr Brazaluk. "Numerical Study of Aerodynamic Characteristics of a Pointed Plate of Variable Elongation in Subsonic and Supersonic Gas Flow." *Journal of Advanced Research in Fluid Mechanics and Thermal Sciences* 96, no. 2 (2022): 88-97. https://doi.org/10.37934/arfmts.96.2.8897